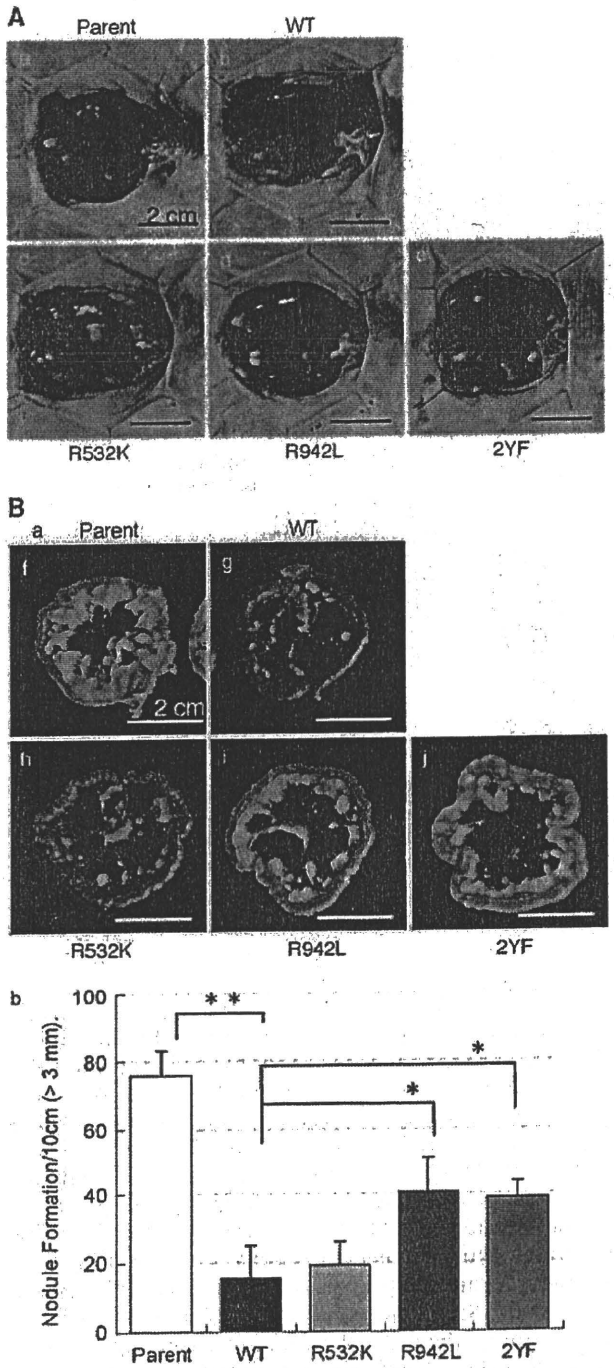

Figure 8 Expression of ARAP3 mutants affects peritoneal dissemination of gastric carcinoma cells. 58As9 cells expressing ARAP3 mutants were injected intraperitoneally into BALB/c nude mice (4×10^6 cells/mouse, $n = 5$). Nineteen days after injection, the R532K mutant ARAP3 suppressed ascites formation and peritoneal dissemination, but the R942L and 2YF mutants did not (**A** and **Ba**). Similarly, R532K also reduced the number of mesentery nodules formed after tumor cell inoculation, whereas R942L and 2YF did not (**Bb**) ($^*P<0.05$ $^{**}P<0.01$).

how the phosphotyrosine-dependent signal of ARAP3 suppresses cell-ECM attachment, migration and invasion of cancer cells.

We also observed that the Arf-GAP domain of ARAP3 regulated the internalization of epidermal growth factor receptor following epidermal growth factor stimulation (data not shown), similar to that reported in ARAP1 (Daniele *et al.*, 2008; Yoon *et al.*, 2008). However, judging from the results in this study, the Arf-GAP activity of ARAP3 does not significantly contribute to the suppression of peritoneal dissemination.

Several suppressors of integrin signaling or cell-ECM adhesion have been identified as possible therapeutic targets for preventing peritoneal dissemination of scirrhous gastric carcinoma (Nishimura *et al.*, 1996; Matsuoka *et al.*, 1998). Likewise, ARAP3, which regulates both cell-ECM adhesion and invasiveness, may be a novel therapeutic target. Small molecules that mimic the suppressive function of ARAP3, induce its expression or promote tyrosine phosphorylation of ARAP3 are anticipated to be effective drugs to prevent peritoneal dissemination of scirrhous gastric carcinoma cells.

Materials and methods

Materials

Anti-ARAP3 antibodies used for western blotting were purchased from Abcam (Cambridge, MA, USA), whereas those used for immunohistochemistry were purchased from Santa Cruz Biotechnology (Santa Cruz, CA, USA). Anti-phosphotyrosine (4G10) antibody was obtained from Upstate Biotechnology (Lake Placid, NY, USA). Sheep antimouse antibodies and sheep antirabbit antibodies were bought from GE Healthcare (Buckinghamshire, UK). Rabbit antigoat antibodies were purchased from Zymed (Carlsbad, CA, USA). Alexa 594-conjugated phalloidin was obtained from Molecular Probes (Carlsbad, CA, USA).

Immunohistochemical staining

Paraffin-embedded tissue samples of human scirrhous or non-scirrhous gastric carcinoma were obtained from the National Cancer Center Hospital (Tokyo, Japan). Sections on glass slides were rehydrated and autoclaved at 120 °C for 10 min to reactivate the antigen. Thereafter, the specimens were immunostained using the indirect polymer method with Envision reagent (Dako, Carlsbad, CA, USA) and ARAP3 antibodies (1:500 dilution). Finally, the stained sections were examined with an Olympus BX51 microscope (Tokyo, Japan).

Cell culture

Gastric cancer cell lines (HSC-39, HSC-43, HSC-44PE, 44As3, HSC-58, 58As1, 58As9, HSC-59, HSC-60, HSC-64, KATO3, NKPS, TMK1 and MKN28) were maintained in RPMI 1640 medium (Sigma, St Louis, MO, USA) supplemented with 10% fetal bovine serum (Equitech-Bio, Kerrville, TX, USA) at 37 °C in a humidified atmosphere containing 5% CO_2. G418 (600 ng/ml; Sigma) or Blasticidin (10 ng/ml; Sigma) were also included in the growth medium to select for ARAP3-over-expressing or knockdown cells, respectively.

Construction of ARAP3 Stealth RNAi, miR RNAi and pDONA1-ARAP3 retroviral vectors.

The ARAP3 gene was subcloned from a pEGFP-ARAP3 plasmid into a pDON-A1 retrovirus vector, and then mutant

ARAP3 plasmids were constructed using the QuickChange Site-Directed Mutagenesis Kit (Stratagene, Cedar Creek, TX, USA).

The miR RNAi design was based on the sequence of Stealth RNAi, which was designed using the BLOCK-iT RNAi designer tool (https://rnaidesigner.invitrogen.com/rnaiexpress/, Invitrogen, Carlsbad, CA, USA).

Phalloidin staining

Gastric cancer cells cultured on coverslips were fixed with 4% paraformaldehyde for 10 min at room temperature. The samples were incubated with 3% bovine serum albumin for 1 h in Tween-Tris buffered saline (TTBS), followed by incubation with Alexa-594-conjugated phalloidin in TTBS for 45 min at room temperature, and coverslips were mounted on glass slides. The samples were examined using an Olympus IX-70 confocal laser-scanning microscope or an Olympus BX51 microscope for fluorescence microscopy. Phalloidin was used at 1:500 dilutions.

Immunoprecipitation and western blotting

Whole-cell lysates of gastric cancer cells were harvested by PLC lysis buffer (50 mM 4-(2-hydroxyethyl)-1-piperazineethanesulfonic acid (pH 7.5), 150 mM NaCl, 1.5 mM $MgCl_2$, 1 mM ethylene glycol tetraacetic acid, 10% glycerol, 100 mM NaF, 1% Triton X-100, 1 mM sodium orthovanadate, 10 μg/ml leupeptin, 10 μg/ml aprotinin and 1 M phenylmethylsulfonyl fluoride), and used for immunoprecipitation and immunoblotting. Equal amounts of total protein were separated by SDS–polyacrylamide gel electrophoresis and transferred to polyvinylidene fluoride membranes. The membranes were incubated with primary antibodies overnight at 4 °C, and then incubated with Horseradish peroxide (HRP)-conjugated secondary antibodies for 45 min at room temperature. Bands were detected on an X-ray film using an enhanced chemiluminescence system (Perkin elmer, Waltham, MA, USA)). Primary antibodies were used at dilutions of 1:1000 for ARAP3, 1:2000 for α-Tubulin and 1:5000 for phosphotyrosine.

Adhesion test

Cultured gastric cancer cell lines were dissociated with Hank's Balanced Salt Solution containing 0.25 mM EDTA. Cell suspensions (5×10^4 cells/well) were seeded into 24-well plates coated with collagen (Nitta gelatin, Osaka, Japan), fibronectin (Sigma) or vitronectin (TaKaRa, Shiga, Japan) according to the manufacturer's procedure. After incubating the plates for 30 min at 37 °C in a humidified atmosphere containing 5% CO_2, unattached cells were removed by washing with PBS, and then attached cells were trypsinized and counted with a Z1Coulter counter (Beckman Coulter, Brea, CA, USA).

Cell migration and invasion assays

Gastric cancer cells were dissociated with Hank's Balanced Salt Solution containing 0.25 mM EDTA. For the cell invasion assay, cell culture inserts (8.0 μM pore) were coated on the top and bottom surfaces with matrigel (10 μg/well) and fibronectin, respectively. In the cell migration assay, only the bottom surface was coated with fibronectin. Cells (2×10^4) suspended in serum-free RPMI1640 medium were seeded into each cell culture insert. These inserts were then transferred to a culture plate containing RPMI1640 medium with 5% FBS. After incubating at 37 °C in a humidified atmosphere containing 5% CO_2 for 8 h (migration assay) or 12 h (invasion assay), the cells were fixed with 4% paraformaldehyde and stained with Giemsa staining solution. Assays were performed in triplicate.

Ex vivo cell adhesion assay

Ten-millimeter square pieces of the peritoneal wall, including the peritoneum and abdominal skeletal muscle, were excised from 5-week-old BALB/c nude mice. The pieces were placed on top of a layer of 3% agarose gel in culture dishes, with the peritoneum side facing up. Equal numbers of parent 44As3 cells or 44As3 ARAP3 miR cells (4×10^6 cells/dish) were seeded onto the peritoneal tissue, and then incubated in RPMI 1640 medium containing 10% FBS, 50 μg/ml gentamicin, penicillin and streptomycin for 4 weeks. Finally, the cultured peritoneal walls were removed, fixed in 4% paraformaldehyde and embedded in paraffin for histological analysis.

Inoculation of gastric tumor cells into nude mice

Gastric cancer cell lines were trypsinized, and aliquots of 4×10^6 cells were injected intraperitoneally into BALB/c nude mice purchased from CLEA Japan (Tokyo, Japan). After 3 weeks, the mice were killed and dissected. These experiments were approved by the Committee for Ethics of Animal Experimentation and conducted in accordance with the Guidelines for Animal Experiments in the National Cancer Center.

Conflict of interest

The authors declare no conflict of interest.

Acknowledgements

The pEGFP-ARAP3 plasmid was a kind gift from Krugmann S (Cambridge, UK). This work was supported by a Grant-in-Aid for Cancer Research and by a Grant-in-Aid for Scientific Research from the Ministry of Education, Culture, Science and Technology of Japan for the Third Term Comprehensive 10-Year Strategy for Cancer Control.

References

Brown MT, Cooper JA. (1996). Regulation, substrates and functions of src. *Biochem Biophys Acta* **1287**: 121–149.

Carragher NO, Frame MC. (2004). Focal adhesion and actin dynamics: a place where kinases and proteases meet to promote invasion. *Trends Cell Biol* **14**: 241–249.

Carramusa L, Ballestrem C, Zilberman Y, Bershadsky AD. (2007). Mammalian diaphanous-related formin Dia1 controls the organization of E-cadherin-mediated cell-cell junctions. *J Cell Sci* **120**: 3870–3882.

Chen TJ, Gehler S, Shaw AE, Bamburg JR, Letourneau PC. (2006). Cdc42 participates in the regulation of ADF/cofilin and retinal growth cone filopodia by brain derived neurotrophic factor. *J Neurobiol* **66**: 103–114.

Daniele T, Di Tullio G, Santoro M, Turacchio G, De Matteis MA. (2008). ARAP1 regulates EGF receptor trafficking and signalling. *Traffic* **9**: 2221–2235.

Faix J, Grosse R. (2006). Staying in shape with formins. *Dev Cell* **10**: 693–706.

Frame MC. (2002). Src in cancer: deregulation and consequences for cell behaviour. *Biochim Biophys Acta* **1602**: 114–130.

Huveneers S, Danen EH. (2009). Adhesion signaling—crosstalk between integrins, Src and Rho. *J Cell Sci* **122**: 1059–1069.

I ST, Nie Z, Stewart A, Najdovska M, Hall NE, He H *et al.* (2004). ARAP3 is transiently tyrosine phosphorylated in cells attaching to fibronectin and inhibits cell spreading in a RhoGAP-dependent manner. *J Cell Sci* **117**: 6071–6084.

Itoh K, Yoshioka K, Akedo H, Uehata M, Ishizaki T, Narumiya S. (1999). An essential part for Rho-associated kinase in the transcellular invasion of tumor cells. *Nat Med* **5**: 221–225.

Kim HS, Bae CD, Park J. (2010). Glutamate receptor-mediated phosphorylation of ezrin/radixin/moesin proteins is implicated in filopodial protrusion of primary cultured hippocampal neuronal cells. *J Neurochem* **113**: 1565–1576.

Kowanetz K, Husnjak K, Holler D, Kowanetz M, Soubeyran P, Hirsch D *et al.* (2004). CIN85 associates with multiple effectors controlling intracellular trafficking of epidermal growth factor receptors. *Mol Biol Cell* **15**: 3155–3166.

Krugmann S, Anderson KE, Ridley SH, Risso N, McGregor A, Coadwell J *et al.* (2002). Identification of ARAP3, a novel PI3K effector regulating both Arf and Rho GTPases, by selective capture on phosphoinositide affinity matrices. *Mol Cell* **9**: 95–108.

Krugmann S, Andrews S, Stephens L, Hawkins PT. (2006). ARAP3 is essential for formation of lamellipodia after growth factor stimulation. *J Cell Sci* **119**: 425–432.

Krugmann S, Williams R, Stephens L, Hawkins PT. (2004). ARAP3 is a PI3K- and rap-regulated GAP for RhoA. *Curr Biol* **14**: 1380–1384.

Matsuoka T, Hirakawa K, Chung YS, Yashiro M, Nishimura S, Sawada T *et al.* (1998). Adhesion polypeptides are useful for the prevention of peritoneal dissemination of gastric cancer. *Clin Exp Metastasis* **16**: 381–388.

Nishimura S, Chung YS, Yashiro M, Inoue T, Sowa M. (1996). Role of alpha 2 beta 1- and alpha 3 beta 1-integrin in the peritoneal implantation of scirrhous gastric carcinoma. *Br J Cancer* **74**: 1406–1412.

Raaijmakers JH, Deneubourg L, Rehmann H, de Koning J, Zhang Z, Krugmann S *et al.* (2007). The PI3K effector Arap3 interacts with the PI(3,4,5)P3 phosphatase SHIP2 in a SAM domain-dependent manner. *Cell Signal* **19**: 1249–1257.

Sarmiento C, Wang W, Dovas A, Yamaguchi H, Sidani M, El-Sibai M *et al.* (2008). WASP family members and formin proteins coordinate regulation of cell protrusions in carcinoma cells. *J Cell Biol* **180**: 1245–1260.

Tanaka M, Sasaki K, Kamata R, Hoshino Y, Yanagihara K, Sakai R. (2009). A novel RNA-binding protein, Ossa/C9orf10, regulates activity of Src kinases to protect cells from oxidative stress-induced apoptosis. *Mol Cell Biol* **29**: 402–413.

Uekita T, Tanaka M, Takigahira M, Miyazawa Y, Nakanishi Y, Kanai Y *et al.* (2008). CUB-domain-containing protein 1 regulates peritoneal dissemination of gastric scirrhous carcinoma. *Am J Pathol* **172**: 1729–1739.

Yanagihara K, Takigahira M, Tanaka H, Komatsu T, Fukumoto H, Koizumi F *et al.* (2005). Development and biological analysis of peritoneal metastasis mouse models for human scirrhous stomach cancer. *Cancer Sci* **96**: 323–332.

Yeatman TJ. (2004). A renaissance for SRC. *Nat Rev Cancer* **4**: 470–480.

Yoon HY, Lee JS, Randazzo PA. (2008). ARAP1 regulates endocytosis of EGFR. *Traffic* **9**: 2236–2252.

Supplementary Information accompanies the paper on the Oncogene website (http://www.nature.com/onc)

THE JOURNAL OF BIOLOGICAL CHEMISTRY VOL. 286, NO. 20, pp. 18251–18260, May 20, 2011

Cancer Susceptibility Polymorphism of p53 at Codon 72 Affects Phosphorylation and Degradation of p53 Protein*[S]

Received for publication, December 14, 2010, and in revised form, March 18, 2011 Published, JBC Papers in Press, March 28, 2011, DOI 10.1074/jbc.M110.208587

Chikako Ozeki,[a,b,c] Yuichiro Sawai,[d,e] Tatsuhiro Shibata,[f] Takashi Kohno,[g] Koji Okamoto,[a,h] Jun Yokota,[g] Fumio Tashiro,[e] Sei-ichi Tanuma,[c] Ryuichi Sakai,[i] Tatsuya Kawase,[a,e] Issay Kitabayashi,[b] Yoichi Taya,[a,j1] and Rieko Ohki[a,d,i2]

From the [a]Radiobiology Division, [b]Molecular Oncology Division, [f]Division of Cancer Genomics, [g]Biology Division, [h]Early Oncogenesis Research Project, [i]Growth Factor Division, [d]Division of Cancer Biology, National Cancer Center Research Institute, Tsukiji 5-1-1, Chuo-ku, Tokyo 104-0045, Japan, the [e]Department of Biological Science and Technology, Faculty of Industrial Science and Technology, [c]Department of Biochemistry, Faculty of Pharmaceutical Sciences, Tokyo University of Science, Yamazaki 2641, Noda-shi, Chiba 270-8510, Japan, and the [j]Cancer Science Institute of Singapore and Department of Biochemistry, National University of Singapore, Center for Life Sciences 02-07, Medical Drive, 117456, Singapore

The common polymorphism of p53 at codon 72, either encoding proline or arginine, has drawn attention as a genetic factor associated with clinical outcome or cancer risk for the last 2 decades. We now show that these two polymorphic variants differ in protein structure, especially within the N-terminal region and, as a consequence, differ in post-translational modification at the N terminus. The arginine form (p53-72R) shows significantly enhanced phosphorylation at Ser-6 and Ser-20 compared with the proline form (p53-72P). We also show diminished Mdm2-mediated degradation of p53-72R compared with p53-72P, which is at least partly brought about by higher levels of phosphorylation at Ser-20 in p53-72R. Furthermore, enhanced p21 expression in p53-72R-expressing cells, which is dependent on phosphorylation at Ser-6, was demonstrated. Differential p21 expression between the variants was also observed upon activation of TGF-β signaling. Collectively, we demonstrate a novel molecular difference and simultaneously suggest a difference in the tumor-suppressing function of the variants.

The *p53* gene is a tumor suppressor gene, and loss of functional p53 is the most common anomaly found in human cancers (1). Signals activated upon various cellular stresses stabilize and activate p53, which exerts its tumor-suppressive function mainly by acting as a transcriptional activator. Target genes of p53 regulate a variety of processes, such as the induction of cell cycle arrest, cell death, DNA repair and senescence, and function downstream of p53 to prevent tumorigenesis (2). Depending on the stress signal, p53 selectively activates its target genes to implement various p53-mediated responses. Post-translational modification of p53 is a candidate mechanism that causes p53 to respond to different stress signals, and phosphorylation of p53 is the most major post-translational modification of p53 (3, 4). Kinases activated upon cellular stress, such as ataxia telangiectasia-mutated (ATM), ataxia telangiectasia and Rad3-related (ATR), and p38, phosphorylate serine and threonine residues, and phosphorylation results in the activation of p53 protein (5).

The structure of p53 protein is commonly divided into three functional domains as follows: the N-terminal domain, central core DNA-binding domain, and C-terminal domain. The N-terminal domain is required for the transcriptional activity of p53 protein and consists of two transactivation domains and a proline-rich domain. The transactivation domains are extensively phosphorylated upon p53 activation. Seven serines, Ser-6, -9, -15, -20, -33, -37, and -46, within the transactivation domain undergo phosphorylation (6). Phosphorylation of each residue has been reported to have specific physiological significance; for example, phosphorylation of Ser-15 or -46 modifies the transactivation ability of p53 (7–9), whereas Ser-20 is required for p53 protein stability (10). When not phosphorylated, p53 is actively degraded by the 26 S proteasome pathway by interacting with a ring finger ubiquitin E3 ligase, Mdm2. Upon activation, p53 is phosphorylated at Thr-18 and Ser-20, both of which reside within the Mdm2 binding domain, leading to reduced affinity with Mdm2 and escape from ubiquitination and subsequent degradation (11).

The proline-rich domain functions as a protein-protein interaction domain, and several proteins that bind to this region have been reported (12, 13). In particular, five *PXXP* motifs appearing in this domain are known to be critical for the interaction with Src homology 3 domain-containing proteins. In addition, within the proline-rich domain, a common polymorphism of p53 at codon 72, encoding either proline or arginine (p53-72P or p53-72R), has been reported (14–16). Notably, the proline at residue 72 of p53 is part of a *PXXP* motif, and

* This work was supported by grants-in-aid for scientific research from the Ministry of Education, Culture, Sports, Science, and Technology of Japan (to R. O., T. K., and Y. T.), grants-in-aid for the Third Term Comprehensive Ten-year Strategy for Cancer Control from the Ministry of Health, Labor, and Welfare Japan (to T. S., J. Y., and Y. T.), Program for Promotion of Fundamental Studies in Health Sciences of the National Institute of Biomedical Innovation (to T. S., T. K., and J. Y.), New Energy and Industrial Technology Development Organization (to R. O.), research grants from Hayashi Memorial Foundation for Female Natural Scientists (to R. O.), the Sagawa Foundation for Promoting Cancer Research (to R. O.), Takeda Science Foundation (to R. O.), Kobayashi Foundation for Cancer Research (to R. O.), and the Mochida Memorial Foundation for Medical and Pharmaceutical Research (to R. O.).

[S] The on-line version of this article (available at http://www.jbc.org) contains supplemental Figs. S1–S6.

[1] To whom correspondence may be addressed. E-mail: csiyt@nus.edu.sag.

[2] To whom correspondence may be addressed. Tel.: 81-3-3542-2511 (Ext. 4304); Fax: 81-3-3542-8170; E-mail: rohki@ncc.go.jp.

therefore it can be assumed that the polymorphism will affect protein-binding partners. Extensive studies have been carried out to investigate the link between the expression of p53 polymorphic variants at codon 72 and cancer susceptibility (17). It has been reported that in a number of cancers, including lung and breast, patients with the p53-72P allele are more susceptible to cancer development and a poor clinical outcome (18–21); however, the mechanistic basis for this bias is still an open question.

To determine the functional difference of the two variant proteins p53-72R and p53-72P, we first analyzed the protease accessibility of p53-72R and p53-72P, and we found that the higher order structures are different between them. We have also found that the phosphorylation modifications of both variants are different, leading to differential protein stability and transactivation ability of the two variants.

EXPERIMENTAL PROCEDURES

Plasmids—For p53 constructs, each p53 was cloned in pcDNA3 or pMX vector as described (22). When cloned in pMX vector, each p53 is under the control of a weak retroviral LTR promoter. Constitutively active TGF-β receptor I was constructed by introducing a point mutation at codon 204 (T204D) and cloned in pcDNA3. FLAG-tagged human wild-type Mdm2 (pSG-F-Hdm2), N-terminally c-Myc tagged Mdm2 (pCMV-Myc-Mdm2), and histidine-tagged ubiquitin expression plasmids were described previously (23).

Expression and Purification of Glutathione S-Transferase (GST) Fusion Proteins—GST fusion constructs of p53-72P and -72R were prepared by PCR tagging of p53 cDNA with BamHI and XhoI sites at the 5′ and 3′ ends, respectively, and subcloned into pGEX-6P-1 vector (Amersham Biosciences). Constructs were expressed in *Escherichia coli* (BL21-Gold (DE3) Competent Cell; Stratagene, CA) and purified from cell lysates using glutathione-Sepharose 4B beads (Amersham Biosciences). Purified proteins were further digested with PreScission protease (Amersham Biosciences) to cleave p53 from GST.

Cell Culture, Transfection, and Establishment of Stable Cell Lines—Cell culture was performed as described (22). Transient transfection assays were performed using Lipofectamine Plus or Lipofectamine 2000 reagent (Invitrogen), as indicated in the figure legends. Stable HCT116 p53(−/−) cell lines expressing p53-72P or -72R were obtained by infecting cells with recombinant retroviruses. In each case, as the control cell line, cells were also infected with empty retroviruses expressing only the drug resistance gene. Infection was performed in the presence of Polybrene (at 4 μg/ml; Sigma), and subsequently, cells were selected in puromycin (at 0.5 μg/ml; Sigma). To avoid possible disadvantages from utilizing clonal cell lines, *i.e.* clonal differences, cell lines were maintained as mass cultures.

Western Blotting Analysis and Immunoprecipitation—Cells were lysed in lysis buffer containing 50 mM Tris-HCl (pH 8.0), 1% Nonidet P-40, 250 mM NaCl, 50 mM NaF, 1 mM Na_3VO_4, 1 mM protease inhibitor (PMSF, aprotinin, and leupeptin), and 1 mM DDT. Whole cell lysates were subjected to protein quantification and subjected to immunoprecipitation or analyzed by Western blotting. The antibodies used in this study were as follows: anti-p53 goat polyclonal antibody (FL393); anti-p21 rabbit polyclonal antibody (C-19); anti-PIG3 (N-20) and PIG3 (C-20) goat polyclonal antibody; anti-Bax (N-20) mouse monoclonal antibody; anti-c-Myc mouse monoclonal antibody (9E10) and anti-β-actin mouse monoclonal antibody (Santa Cruz Biotechnology, Santa Cruz, CA); penta-His antibody (Qiagen, Valencia, CA); anti-p53 mouse monoclonal antibodies PAb1801 and PAb421 and anti-Mdm2 mouse monoclonal antibody (clone IF-2) (Calbiochem); anti-p53 mouse monoclonal antibody (PAb122) (Monosan, Uden, Netherlands); anti-phospho-p53 (Ser-6, -9, -15, -20, -37, and -46) rabbit polyclonal antibodies and anti-phospho-Smad2 (138D4) Ser-465/467 antibody (Cell Signaling, Beverly, MA); anti-CRP1 antibody (BD Transduction Laboratories); and anti-FLAG mouse monoclonal antibody (M2); and anti-tubulin antibody (clone B-5-1-2) (Sigma). To detect total p53, anti-p53 goat polyclonal antibody (FL393) was used in all cases.

Northern Blotting Analysis—RNA was prepared using an RNeasy Midi kit (Qiagen). Northern blotting was performed as described (22). Probes were prepared using a BcaBEST labeling kit (TaKaRa, Kyoto, Japan) and purified by serial purification using a Probe Quant G-50 MicroColumn (Amersham Biosciences) and NICK column (Amersham Biosciences). The full open reading frame of p53 was used for probe preparation.

Detection of Ubiquitinated p53—To detect efficiently the ubiquitinated p53, Mdm2 expression vector pSG-FLAG-Mdm2 was used, in which Mdm2 was expressed from an SV40 promoter (much weaker than CMV promoter). pcDNA3-p53-72P or -72R (0.35 μg), together with His_6-tagged ubiquitin (2.2 μg) and N-terminally FLAG-tagged Mdm2 (pSG-FLAG-Mdm2, 1.42 μg) or control empty vector (1.42 μg), were introduced into H1299 cells (6×10^5 cells/10-cm dish). Cells were harvested 27 h post-transfection. Cell lysates were prepared in the presence of 1 mg/ml *N*-methylmaleimide (Sigma) to avoid degradation of ubiquitinated p53. Ubiquitinated and nonubiquitinated p53 were immunoprecipitated with anti-p53 polyclonal antibody (FL393) and analyzed by Western blotting.

^{35}S Pulse-Chase—H1299 cells (4×10^5 cells/10-cm dish) were transfected with 4 μg of plasmids with a 1:9 ratio of pcDNA-p53-72P or 72R/pCMV-Myc-Mdm2. At 19.5 h after transfection, cells were starved for 30 min in methionine- and cysteine-free DMEM with dialyzed serum and then labeled with 4.1 MBq/ml EXPRE^{35}S^{35}S ^{35}S-protein labeling mix (PerkinElmer Life Sciences) for 30 min. Cells were then cultured for 1.5 h in chase medium containing 500 μg/ml methionine and 500 μg/ml cysteine. Following incubation, cells were collected at the indicated times. Whole cell lysates were prepared from the collected cells, and immunoprecipitation was performed using anti-p53 mouse monoclonal antibodies PAb1801 and PAb421, run on SDS-PAGE, and detected by autoradiography.

Analysis of p53 Single Nucleotide Polymorphism and the Copy Number of the mdm2 Gene by Array-based Comparative Genomic Hybridization—To analyze p53 single nucleotide polymorphisms, a 10- or 20-ml whole blood sample was obtained from each individual. Genomic DNA was isolated and subjected to genotyping for p53 single nucleotide polymorphism by pyrosequencing, as described previously (19). For

array-based comparative genomic hybridization, 62 surgical specimens of lung cancer patients who had been diagnosed and had undergone surgery at the National Cancer Center Hospital were analyzed by MCG cancer array-800 comparative genomic hybridization, as described previously (24). MCG Cancer array-800 is a custom-made array consisting of ~800 BACs harboring 800 known cancer-related genes, intended for diagnosis of cancer-specific copy number aberrations. When the signal ratio (test signal/reference signal) for the copy number of the *mdm2* gene was more than 1.25, it was defined as chromosomal gain. The threshold for chromosomal gain (ratio >1.25) was determined previously by "normal *versus* normal experiments" (24).

RESULTS

N-terminal Structures of p53-72P and -72R Protein Are Different—The polymorphism of p53 at codon 72 was first reported over 2 decades ago as a non-tumor-derived amino acid change that altered the mobility of p53 on SDS-polyacrylamide gels (14–16). As shown in supplemental Fig. S1, *A* and *B*, altered mobilities of ectopically expressed, endogenously expressed, and purified p53-72P and -72R were similarly detected by Western blotting. Because purified p53 proteins prepared from *E. coli* do not undergo post-translational modifications (data not shown), the altered mobility is not due to such modifications but to the intrinsic nature of the proteins. It has been suggested that this altered mobility reflects the altered structure of the protein by amino acid change; however, because structural information about this domain is lacking, this hypothesis has not been tested. We therefore tried to test this hypothesis by partial proteolytic digestion of purified p53-72P and -72R protein. When a protein is partially digested by proteases, a difference in the protein structure is detected as sensitivity to protease digestion at each cleavage site. To observe intrinsic differences between p53-72P and -72R proteins, we used purified proteins prepared from *E. coli*. As shown in Fig. 1*A*, the products of partial proteolysis by subtilisin were analyzed by Western blotting using anti-p53 antibodies, detecting different positions within the p53 protein. We first recognized that fragments showing altered mobility between p53-72P and -72R were detected even after proteolytic digestion (Fig. 1*A*, *open circles*). Such fragments were frequently detected by the antibody detecting N-terminal p53 (Pab1801), and this demonstrates that N-terminal fragments contain a region causing electrophoretic mobility differences. However, when the antibody detecting C-terminal p53 was used (Pab122), most fragments showed the same migration, showing that the C-terminal portion of p53-72P and -72R is indistinguishable by SDS-PAGE. In addition to these fragments, the analysis revealed two bands detected only in p53-72R (Fig. 1*A*, 22- and 34-kDa bands, shown with *arrows*). As shown in Fig. 1*B*, most of the estimated digestion sites for these bands lie within the N-terminal half of p53, demonstrating that a difference in protease accessibility is frequently observed in the N-terminal p53. We also performed the same experiment using Pab240 (which detects 211–220 amino acids of p53 protein), and we found that the 22-kDa band is not detected by Pab240, suggesting the N-terminal origin of the fragment (data not shown). Unfortunately, several bands appeared around 34 kDa, and we could not verify whether a

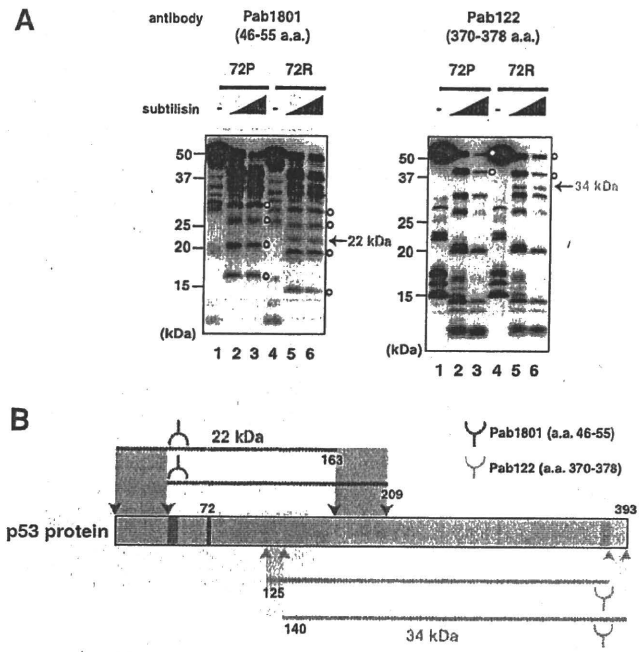

FIGURE 1. **Partial proteolytic digestion of purified p53-72P and -72R.** *A*, 35 ng of purified p53-72P or -72R were digested with subtilisin at 0.5 μg/ml (*lanes 2* and *5*) and at 1 μg/ml (*lanes 3* and *6*) for 30 min on ice. Products were resolved by 15–25% SDS-PAGE and analyzed by Western blotting using the indicated antibodies. Bands with a different proteolytic pattern (specifically observed for p53-72R) are shown by *arrows*. Note that when using antibody against N-terminal positions of p53 (Pab1801), fragments showing altered mobility on the gel between p53-72P and -72R are frequently detected (*open circles*). *B*, estimated digestion sites for p53-72R-specific bands. Schematic representation of p53 protein (*gray*) together with recognition sites for Pab1801 (*green*) and Pab122 (*yellow*) is shown. Polymorphic codon 72 is shown in *red*. The *upper two green bars* (22-kDa band in *panel Pab1801*) and *lower two yellow bars* (34-kDa band in *panel Pab122*) are the estimated alignments of p53-72R-specific fragments. The estimated amino acid numbers of the fragments were calculated according to the molecular weight of the fragments. The fragments were detected by antibodies and therefore should be derived from somewhere between the two bars. It can be assumed that p53-72R-specific digestion occurred between the *arrowheads*.

34-kDa p53-72R-specific band is detected by Pab240 (data not shown). These results collectively indicate that differences in protein structure are mainly detected in the N-terminal portion of p53.

Phosphorylation in N-terminal p53 Is Enhanced in p53-72R Compared with -72P—We next speculated that the difference in the protein structure between the variants might affect the association with the kinases that phosphorylate p53. Because the structural differences of p53-72P and -72R are mainly detected in the N-terminal region, we analyzed the phosphorylation levels of p53-72P and -72R within the N-terminal domain. We reasoned that subtle differences between the variants become evident only when they are expressed within cells having the same genetic background; therefore, we analyzed the phosphorylation levels of p53-72P and -72R by transfecting them into a cell line with no p53 (Saos2 cells). In addition, to exclude the possibility that p53 expressed in the cells is unnaturally high, each p53 was expressed from a weak retroviral LTR promoter. As shown in Fig. 2, phosphorylation levels of p53-72P and -72R were similar on Ser-9, -15, -37, and -46. However, significantly enhanced phosphorylation of 72R compared with 72P at Ser-6 and -20 was detected. Phosphorylation in the

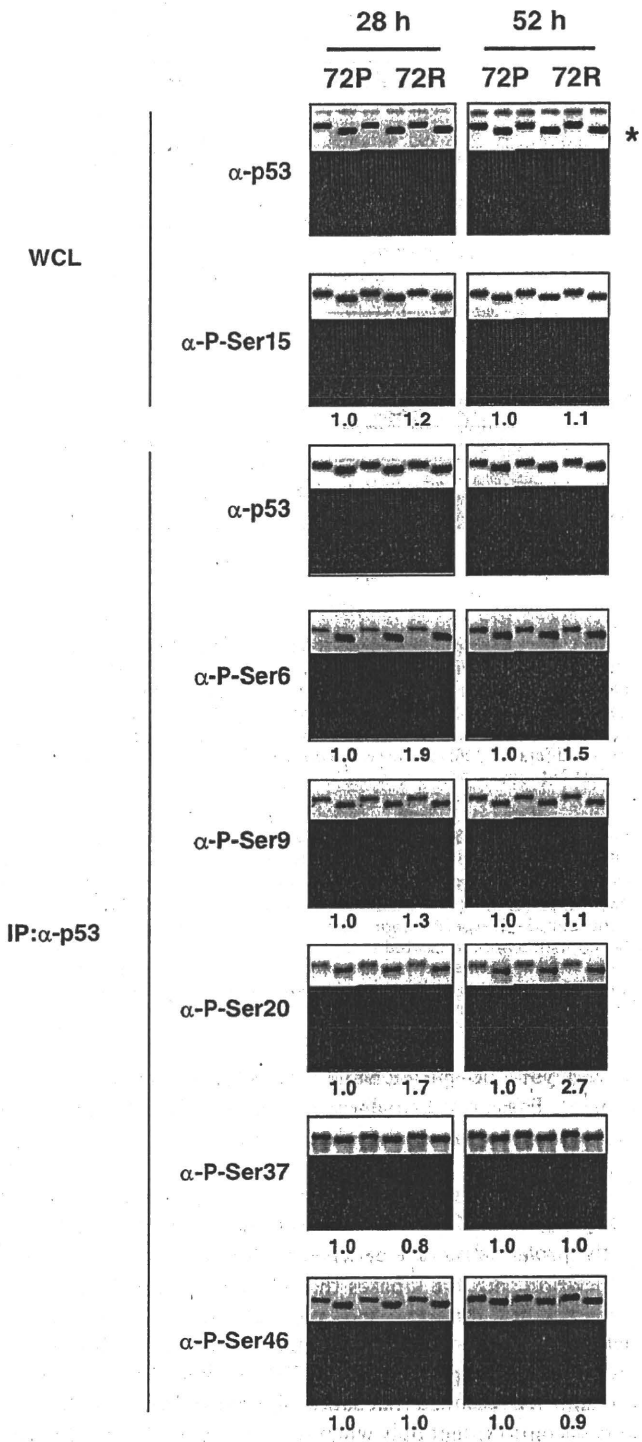

FIGURE 2. **Phosphorylation of p53-72P and -72R within the N-terminal transactivation domain.** Saos2 cells (4.4×10^6 cells/10-cm dish) were transfected with pMX-p53-72P or -72R (1.78 μg), and harvested 28 and 52 h post-transfection. To detect the phosphorylation of p53 efficiently (except Ser-15), p53 proteins were immunoprecipitated (*IP*) using anti-p53 antibodies (anti-p53 mouse monoclonal antibody pAb1801 and pAb421 were mixed). Total p53 and phosphorylated p53 were analyzed by Western blotting. The experiment was repeated three times, and representative images are shown. The phosphorylation levels of p53-72P and -72R were quantified using Image J software. Relative phosphorylation levels (normalized by total p53) are shown *below* the panels. *Asterisk* denotes a nonspecific band. *WCL*, whole cell lysate.

N-terminal region of p53 is closely related with p53 activity. We therefore analyzed whether enhanced phosphorylation at Ser-6 and -20 in p53-72R results in enhanced tumor-suppressing function of the protein, as shown below.

Stability of p53-72R Is Increased Compared with p53-72P—Phosphorylation at Ser-20 mediates the stabilization of the p53 protein by inhibiting p53-Mdm2 interaction (11). Because we detected enhanced phosphorylation at Ser-20 in p53-72R compared with p53-72P, we focused on the stability of p53 proteins expressed within the cell. We first expressed the variants at different expression levels (200–1200 ng of p53 expression vectors transfected per 10-cm dish). We speculated that if the differences in protein levels were due to differences in degradation levels by endogenous Mdm2, increased expression of p53 would override degradation by Mdm2. As shown in Fig. 3*A*, when both p53s were expressed at relatively high levels (800 or 1200 ng of p53 expression vectors transfected per 10-cm dish), no difference in total p53 levels was detected, whereas when the expression levels were decreased (200 or 400 ng transfected), p53-72R was expressed at a significantly higher level than p53-72P. The mRNA expression levels of both variants were similar even when p53-72R protein was expressed at a significantly higher level than p53-72P protein in H1299 and Saos2 cells (Fig. 3*B*); therefore, the difference in the p53 protein amount is regulated at the post-transcriptional level. We further tested whether this difference could be detected in cells lacking Mdm2. We utilized *p53* and *mdm2* double-deficient mouse embryonic fibroblasts (*p53/mdm2* DKO)[3] for this purpose. As shown in Fig. 3*C*, no difference in p53 protein levels was detected in *p53/mdm2* DKO (under the conditions utilized, expression levels of p53 variants were similar or lower than in H1299 cells, data not shown).

We next tested whether the difference in protein expression levels was affected by phosphorylation at Ser-20, which was converted to alanine in p53-72P and -72R to obtain nonphosphorylatable p53 at Ser-20 (therefore is degradable by Mdm2), and expressed in H1299 and *p53/mdm2* DKO. As shown in Fig. 3*D*, significant decreases in protein levels were detected for S20A mutants compared with wild-type p53s in H1299 cells. However, no such decreases were detected in *p53/mdm2* DKO, indicating that diminished expression levels of S20A mutants in H1299 is a result of enhanced degradation of the mutants by Mdm2. The level of S20A mutant for p53-72P was still slightly lower than p53-72R in H1299 cells, demonstrating that, in addition to phosphorylation at Ser-20, other factors may affect the difference in protein expression levels. Collectively, these results suggest that the difference in p53 protein expression levels is the result of a difference in the degradation levels of p53-72R and -72P by Mdm2, and this difference has been brought about at least partly from differences in phosphorylation levels at Ser-20.

Mdm2 Degrades p53-72P More Efficiently than p53-72R—We further tested whether there is a difference in protein degradation by Mdm2 between polymorphic variants. We first co-transfected Mdm2 with p53-72R or -72P in H1299 cells. As

[3] The abbreviations used are: DKO, double KO; ca., constitutively active.

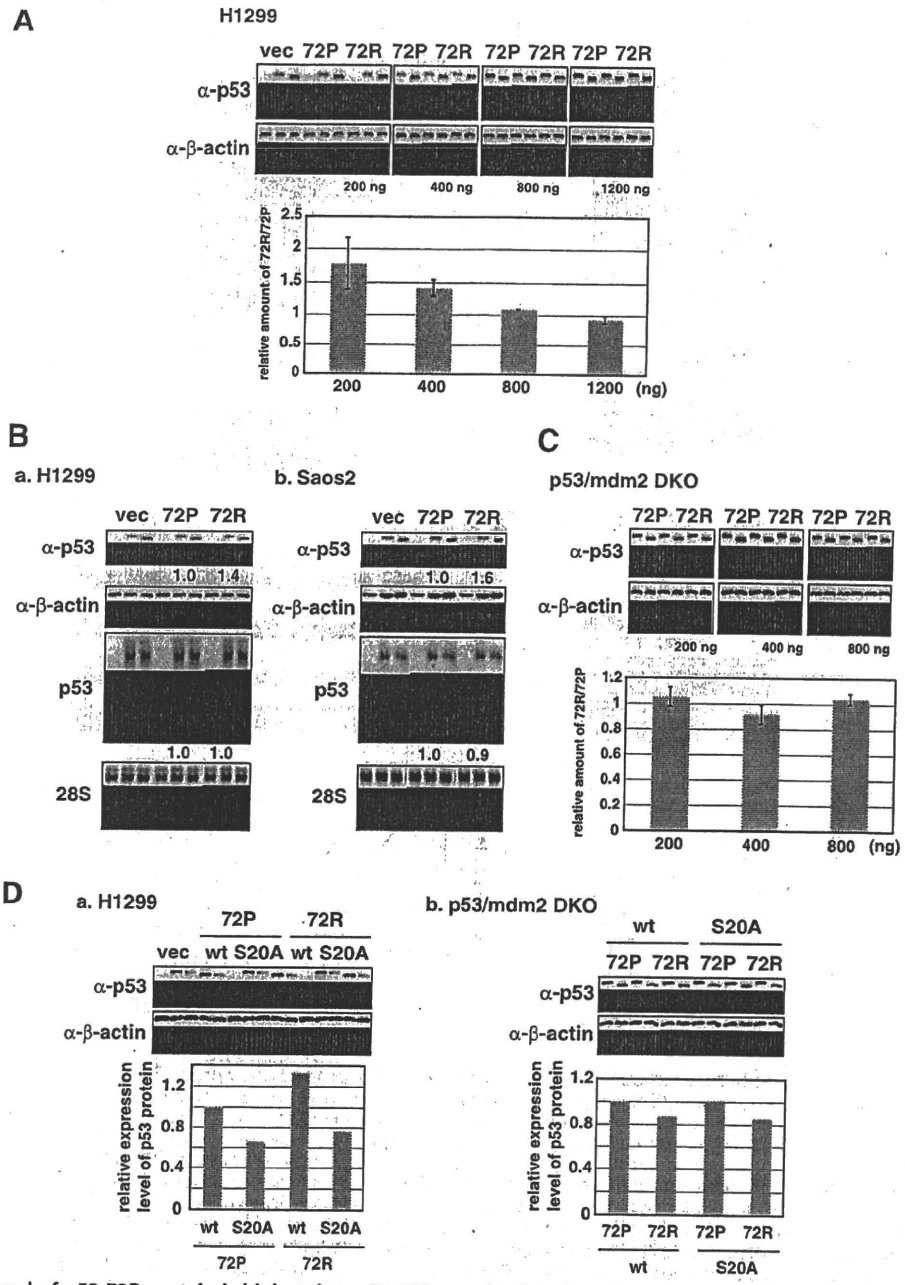

FIGURE 3. **Expression level of p53-72R protein is higher than p53-72P protein.** *A*, indicated amounts of pMX-p53-72P or -72R expression plasmids were introduced into H1299 cells (4.4 × 10^5 cells/10-cm dish). Cells were harvested 27 h post-transfection and analyzed by Western blotting. Experiments were performed in triplicate, and representative images are shown. The levels of p53 and β-actin were quantified using Image J software, and p53 levels were normalized by β-actin levels. The mean ± S.D. of relative p53-72R/p53-72P levels was calculated and is shown in the *bottom column*. *vec*, vector. *B*, p53 protein and mRNA levels were analyzed by Western and Northern blotting. The levels of p53 protein (normalized by β-actin levels) and mRNA (normalized by 28 S levels) were quantified using Image J software. *Panel a*, pMX-p53-72P or -72R (0.2 μg) was introduced into H1299 (4.4 × 10^5 cells/10-cm dish). Cells were harvested 27 h post-transfection. *Panel b*, pMX-p53-72P or -72R (0.9 μg) was introduced into Saos2 cells (4.4 × 10^6 cells/10-cm dish). Cells were harvested 24 h post-transfection. *C*, indicated amounts of pMX-p53-72P or -72R expression plasmids were introduced into *p53/mdm2* DKO (4.4 × 10^5 cells/10-cm dish) and analyzed as in *A*. *D*, expression plasmids (cloned in pMX vector) of wild-type or mutant (S20A) p53-72P or -72R were introduced into H1299 (in *panel a*, 4.4 × 10^5 cells/10-cm dish, 500 ng transfected) or *p53/mdm2* DKO (in *panel b*, 4.4 × 10^5 cells/10-cm dish, 200 ng transfected) cells. Cells were harvested 21 h (*panel a*) or 27 h (*panel b*) post-transfection. Experiments were performed in duplicate, and the mean values of relative p53-72P and -72R levels are presented.

shown in Fig. 4*A*, although p53-72P was efficiently degraded under the conditions tested, p53-72R was resistant to degradation. We further analyzed the ubiquitination of both variants by Mdm2. His-tagged ubiquitin was co-expressed with p53 and Mdm2 in H1299 cells. Cell lysates were prepared, and p53 was immunoprecipitated by anti-p53 antibody. Immunoprecipitates were analyzed by Western blotting using anti-His tag antibody. As shown in Fig. 4*B*, it was shown that His-tagged ubiquitinated p53 was more prominent in p53-72P than p53-72R. We also performed a nickel pulldown assay under denaturing conditions to purify His-tagged ubiquitinated proteins. The samples were then analyzed by Western blotting using anti-p53

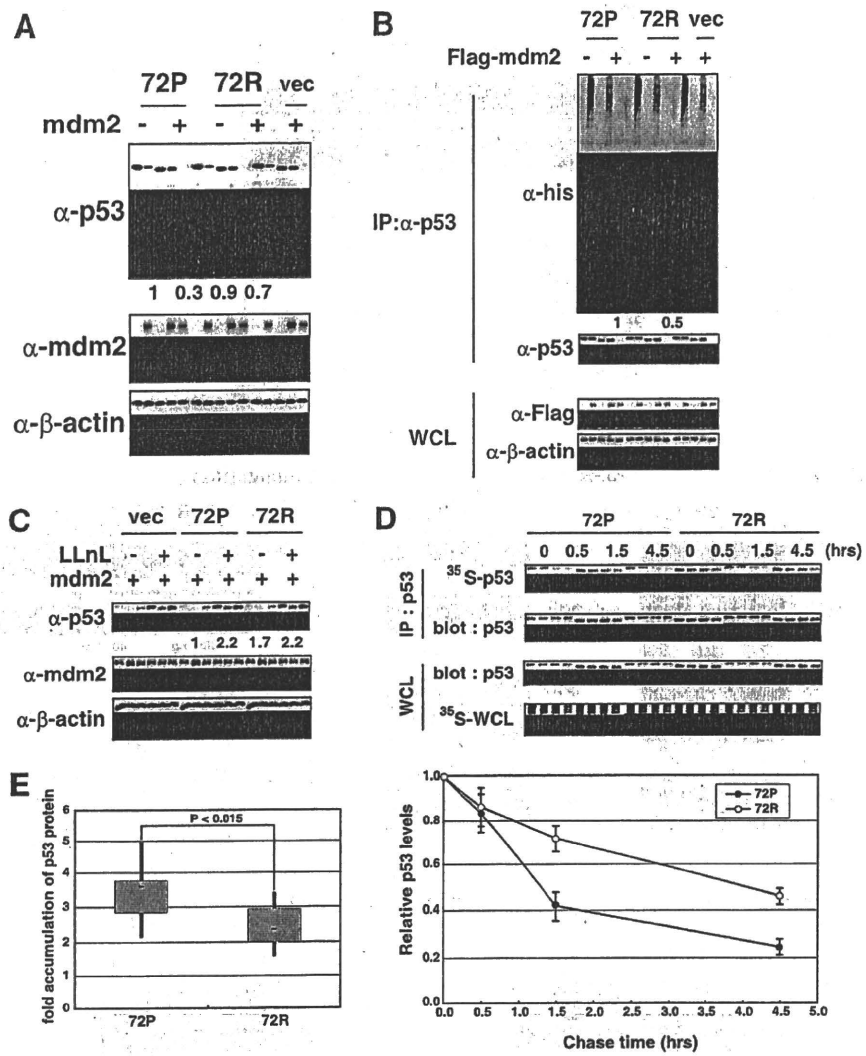

FIGURE 4. **Degradation of p53-72P by Mdm2 is accelerated compared with p53-72R.** *A*, pcDNA3-p53-72P or -72R together with N-terminally c-Myc-tagged Mdm2 (pCMV-Myc-Mdm2; Mdm2 expressed from a CMV promoter) or control empty vector were introduced into H1299 cells (4.4×10^5 cells/10-cm dish) and analyzed by Western blotting. 0.44 μg of p53 and 4 μg of Mdm2 were transfected. Cells were harvested 21 h post-transfection. Levels of p53 (normalized by β-actin) were quantified and are shown *below* the panels. *B*, pcDNA3-p53-72P or -72R (0.35 μg) together with His_6-tagged ubiquitin (2.2 μg) and N-terminally FLAG-tagged Mdm2 (pSG-FLAG-Hdm2, 1.42 μg) or control empty vector (*vec*) (1.42 μg) were introduced into H1299 cells (6×10^5 cells/10-cm dish), and cells were harvested 27 h post-transfection. To detect ubiquitinated p53 efficiently, Mdm2 was expressed at a low level using expression plasmid pSG-F-Hdm2 (Hdm2 is under the control of SV40 promoter, which is much weaker than CMV promoter). p53 was immunoprecipitated (*IP*) with anti-p53 polyclonal antibody (FL393), and immunoprecipitated samples and whole cell lysates (*WCL*) were analyzed by Western blotting. Western blot analyses of immunoprecipitates were performed with the anti-His antibody to detect ubiquitinated p53 (*upper panel*) or with FL393 antibody to detect nonubiquitinated p53 (*lower panel*). Levels of ubiquitinated p53 (normalized by nonubiquitinated p53) were quantified and are shown *below* the panels. *C*, pMX-p53-72P or -72R (0.5 μg) together with pCMV-Myc-Mdm2 (4.5 μg) or control empty vector (4.5 μg) were introduced into H1299 cells (4.4×10^5 cells/10-cm dish). Where indicated, cells were treated with LLnL (50 μM) 16 h post-transfection. Cells were harvested 21 h post-transfection and analyzed by Western blotting. Experiments were performed in triplicate, and representative images are shown. Levels of p53 were quantified (normalized by β-actin) and the relative p53-72P and -72R levels are shown *below* the panel. *D*, pcDNA3-p53-72P or -72R (0.4 μg) together with pCMV-Myc-Mdm2 (3.6 μg) were introduced into H1299 cells (4×10^5 cells/10-cm dish). Cells were pulse-labeled 20 h post-transfection for 30 min and then cultured in chase medium for 1.5 h. Following incubation, cells were harvested at the indicated time points. p53 was immunoprecipitated, and the levels of labeled p53 were detected by autoradiography. Total p53 protein levels were analyzed by Western blotting. Experiments were performed in triplicate, and representative images are shown. Levels of p53 were quantified (normalized by total p53) and the relative p53-72P and -72R levels are shown *below* the panel. *E*, immortalized peripheral lymphocytes from healthy donors were subjected to LLnL treatment. Cells derived from 10 homozygotes each for p53-72P and -72R were subjected to analysis. Each sample was run in triplicate and analyzed by Western blotting (supplemental Fig. S3). Quantification was performed using Image J software. Fold accumulation of p53 protein after LLnL treatment was calculated for each sample and shown as a *box plot*.

antibody to detect the amount of His-tagged ubiquitinated p53s. Again, ubiqitination was more prominent in p53-72P than p53-72R (supplemental Fig. S2).

To further test whether the variants differ in degradation levels mediated by the proteasome pathway, we treated cells co-expressing Mdm2 and p53-72R or -72P with LLnL, a proteasome inhibitor. As shown in Fig. 4*C*, the p53-72P level was significantly increased by LLnL treatment compared with p53-72R, showing that p53-72P is more susceptible to degradation by the proteasome pathway. In addition, both variants were expressed at similar levels after LLnL treatment, supporting the idea that differences in the expression levels of both variant

TABLE 1
Over-representation of p53–72P homozygotes in lung cancer cases with gains of the *mdm2* gene in their tumors

p53 genotype	No. of cases: MDM2 normal	MDM2 gain[a]	Odd ratio (95% confidence interval)	*p* value by Fisher's exact test
	%	%		
R/R + R/P	48 (94)	19 (79)	Reference	
P/P	3 (6)	5 (21)	4.21 (0.94–22.2)	0.101

[a] Copy number ratio >1.25 in tumors by array comparative genomic hybridization analysis using MCG Cancer array-800.

proteins were the result of proteasomal degradation. We also performed [^{35}S]methionine pulse-chase experiments to determine the half-lives of p53 variant proteins. Cells co-expressing Mdm2 and p53-72R or -72P were pulse-labeled, and p53 protein levels were monitored for 4.5 h. As shown in Fig. 4*D*, the half-life of p53-72R was significantly longer than p53-72P, demonstrating that p53-72R is more resistant to Mdm2-mediated degradation.

We next utilized peripheral lymphocytes immortalized using Epstein-Barr virus to analyze the degradation of endogenously expressed p53 proteins. We selected 10 cells each that were homozygous for p53-72P or -72R. To minimize the difference between cell lines, they were also selected based on the criteria that they were derived from healthy donors who were Japanese, male, nonsmoking, and aged 30–50 years old. As shown in supplemental Fig. S3 and Fig. 4*E*, when cells were treated with LLnL, accumulation of p53 protein was more pronounced in cells with p53-72P, confirming the result obtained for exogenously expressed p53 proteins. Collectively, it was shown that ubiquitination by Mdm2 and subsequent degradation is more enhanced in p53-72P than -72R.

Cancer Patients Carrying p53-72P Are Over-represented in Patients with Gain in the mdm2 Gene—The nature of p53-72P being more sensitive to degradation by Mdm2 than p53-72R raises the possibility that homozygotes for the p53-72P allele are more susceptible to developing cancer by up-regulation of Mdm2 expression. We therefore analyzed the copy number of the *mdm2* gene in tumors in combination with genotypes for the p53 polymorphism at codon 72 in the germ line. Seventy five lung cancer cases, consisting of 39 adenocarcinomas, 2 bronchioalveolar carcinomas, 25 squamous cell carcinomas, 2 small cell lung carcinomas, 7 large cell neuroendocrine carcinoma cases, that were available for information both on p53 genotypes in their peripheral blood cells and the *mdm2* gene copy numbers in their tumor cells were subjected to analysis (Table 1). These cases were selected from a Japanese population of lung cancer cases that showed a frequency of the p53-72P allele higher than control individuals in a previous case-control study based on the criterion that information on the *mdm2* gene copy numbers in their tumor was available (19). In fact, the frequency of the p53-72P allele in these 75 cases (*i.e.* 0.41) was higher than that of controls (*i.e.* 0.33), although the difference did not reach statistical significance ($p = 0.070$ by Fisher's exact test). Among the 75 cases, 24 (32%) showed gain of the *mdm2* gene (ratio of test signal/reference signal >1.25) in their tumors. The fraction of p53-72P homozygotes was notably higher in patients with *mdm2* gains in their tumors than without (21 *versus* 6%, $p = 0.101$ by Fisher's exact test). Although further study is required with more test cases, these data suggest that p53-72P individuals develop lung cancer at a higher frequency upon increase of the *mdm2* gene copy number and support our results showing that p53-72P is more susceptible to Mdm2-mediated degradation.

Phosphorylation of Ser-6 Is More Enhanced in p53-72R than -72P under Basal and Damaged Conditions—Ser-6, Ser-15. and Thr-18 are the phosphorylation sites within the N-terminal transactivation domain that are conserved among vertebrates. Phosphorylation of Ser-15 and Thr-18 plays important roles in the regulation of p53 activity; however, although it has been reported that Ser-6 is phosphorylated under damaged or basal conditions, the biological significance of Ser-6 phosphorylation remains elusive (6). Because we found that Ser-6 is strongly phosphorylated in p53-72R compared with p53-72P in Saos2 cells (Fig. 2), we further analyzed under which conditions Ser-6 is phosphorylated. As shown in Fig. 5*A*, upon γ-ray irradiation, the Ser-6 phosphorylation level is increased, and p53-72R is phosphorylated at a higher level than p53-72P in Saos2 cells. In this experiment, the difference in Ser-6 phosphorylation without DNA damage was also confirmed. Under the same conditions, phosphorylation of Ser-15 was induced upon γ-ray irradiation, but no difference was detected between variants with or without γ-ray irradiation. To further analyze p53 phosphorylation under damaged conditions, we obtained cell lines stably expressing both p53s in HCT116 p53(−/−) cells. As shown in supplemental Fig. S4*A*, both cell lines expressed p53-72R or -72P at similar levels and induced p21 upon DNA damage, showing a normal p53 response in these cell lines. Using these cell lines, phosphorylation of Ser-6 under basal conditions and upon DNA damage was analyzed. As shown in Fig. 5*B* and supplemental Fig. S4, *B* and *C* upon γ-ray or UV irradiation, adriamycin or 5-fluorouracil treatment resulted in increased Ser-6 phosphorylation, and under all conditions, p53-72R showed elevated phosphorylation levels compared with p53-72P. Again, phosphorylation of Ser-15 was induced upon γ-ray irradiation, but no difference was detected between variants (Fig. 5*B*).

Phosphorylation of Ser-6 Is Required for p53 Transactivation under Basal Conditions and upon Activation of TGF-β Signaling—To analyze the biological function of Ser-6 phosphorylation, we constructed p53 mutants carrying Ser to Ala conversions at codon 6. Wild-type as well as mutant p53s were expressed in H1299 cells, and the induction of representative p53 target gene products (p21, Bax, PIG-3, and Mdm2) were analyzed by Western blotting. As shown in Fig. 5*C*, all four p53 target gene products were induced by wild-type p53 as expected. Interestingly, wild-type p53 induced p21 more effectively than S6A mutant, demonstrating the involvement of Ser-6 phosphorylation in p21 induction. In addition, as shown in Fig. 5*D*, p53-72R induced p21 more strongly than p53-72P, likely reflecting the difference in Ser-6 phosphorylation levels between proteins. The elevated expression of p21 in p53-72R-expressing cells was also demonstrated in HCT116 p53(−/−) cells stably expressing p53-72P or -72R and in immortalized human peripheral lymphocytes (supplemental Figs. S4*A* and S5*A*).

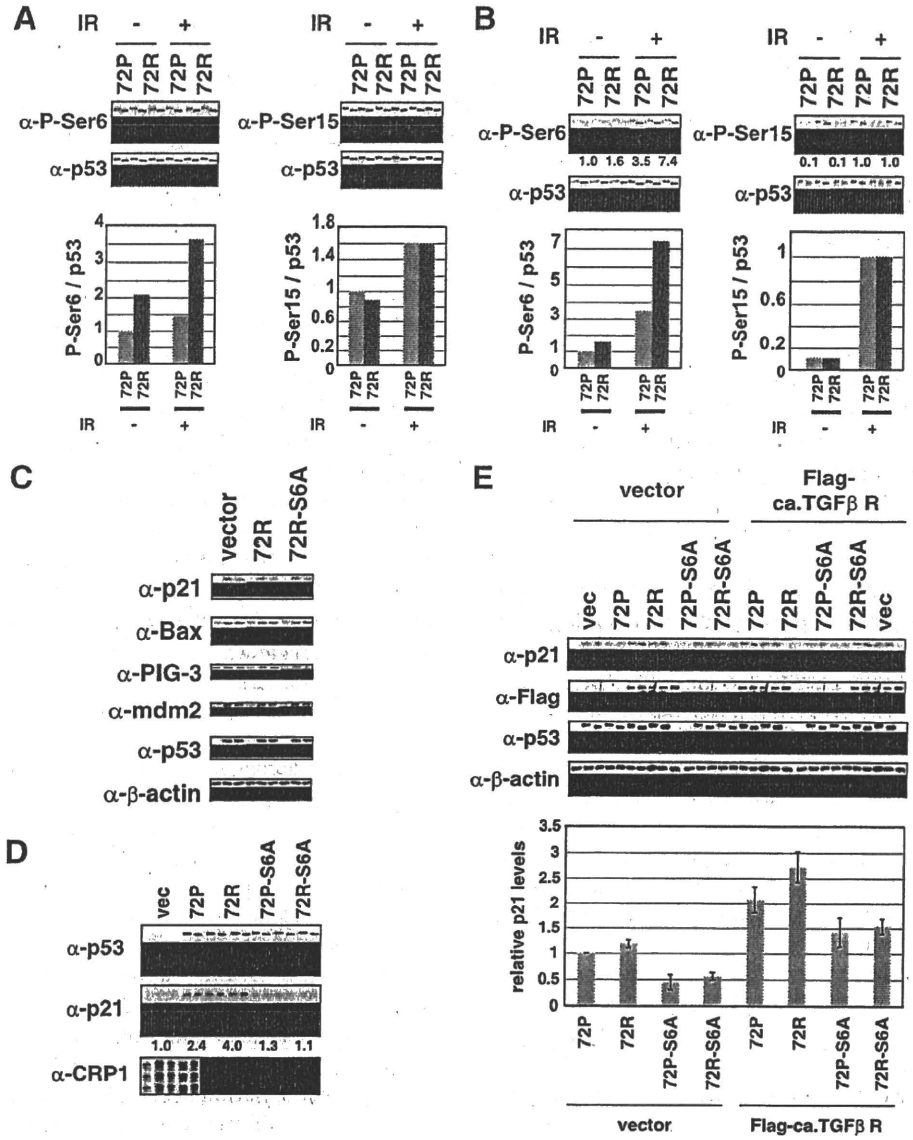

FIGURE 5. **Phosphorylation of p53 at Ser-6 was enhanced in p53-72R compared with -72P, and p53-dependent p21 expression was enhanced in cells expressing p53-72R.** *A*, phosphorylation of p53 at Ser-6 and Ser-15 in Saos2 cells expressing p53-72P or -72R was analyzed by Western blotting. Cells (2.2×10^6 cells/10-cm dish) were transfected with pMX-p53-72P or -72R, treated with γ-ray (20 gray) 24 h post-transfection, and harvested 50 h post-transfection. As in Fig. 2, p53 proteins were immunoprecipitated and analyzed using anti-phospho-Ser-6 p53 antibody (*upper panel*) and anti-p53 antibody (*lower panel*). Levels of phospho-Ser-15 are shown for comparison. To detect phospho-Ser-15 and total p53 in *right panels*, whole cell lysates were analyzed by Western blotting. Relative phosphorylation levels (normalized by total p53 levels) are shown *below* the panels. *B*, HCT116 p53(−/−) cells stably expressing p53-72P or -72R (6.7×10^6 cells/10-cm dish) were treated with γ-ray (20 gray), and cells were harvested 2 h post-irradiation. Levels of phospho-Ser-6 and -15 were analyzed as in *A*. *C*, H1299 cells (4×10^5 cells/10-cm dish) were transfected with pMX-p53-72R or 72R-S6A mutant (0.3 μg) together with pcDNA3 (2.7 μg). Cells were harvested 26 h post-transfection, and analyzed by Western blotting. *D*, wild-type or mutant (S6A) pMX-p53-72P or -72R (1.63 μg) was introduced into H1299 cells (2.4×10^6 cells/10-cm dish), and cells were harvested 29 h post-transfection. Expression of p53, p21, and cytoskeletal CRP1 (as a loading control) was analyzed by Western blotting. The experiment was performed with p53-72P and -72R expressed at similar levels. The levels of p21 and 23-kDa CRP1 were quantified using Image J software, and p21 levels were normalized by CRP1 levels. *E*, H1299 cells (2.4×10^6 cells/10-cm dish) were transfected with pMX-p53-72P or 72R (1.63 μg) and ca. TGF-βR (6.54 μg). Cells were harvested 29 h post-transfection. Expression of ca. TGF-βR was detected by anti-FLAG antibody. Experiments were performed in triplicate, and representative images are shown. The levels of p21 (normalized by β-actin) were quantified using Image J software. The mean ± S.D. of p21 levels was calculated and is shown in the *bottom column*.

It has been reported that the activation of MAPK promotes the phosphorylation of p53 at Ser-6 and Ser-9 (25). Phosphorylation at these sites facilitates the interaction of p53 with activated Smad2 or Smad3 and the subsequent recruitment of p53-Smad2/3 complexes to TGF-β-responsive target promoters (25). As shown in supplemental Fig. S4*D*, we also have confirmed MAPK-dependent phosphorylation of p53 at Ser-6. It has also been shown using H1299 cells that the expression of p53 with amino acid conversions from Ser to Ala at codon 6 or 9 impaired the ability of p53 to enhance TGF-β-mediated expression of the p21 gene (25). Because we detected a significant difference in Ser-6 phosphorylation between the variants, we analyzed whether TGF-β-mediated expression of the p21 gene differs between them. We analyzed TGF-β-dependent up-regulation of p21 by introducing constitutively active TGF-β receptor I (ca. TGF-βR) with p53 variants. It was confirmed

that introduction of ca. TGF-βR results in activation of the TGF-β pathway in H1299 cells, as judged from Smad2 phosphorylation (supplemental Fig. S5*B*). As shown in supplemental Fig. S5*B* and Fig. 5*E*, without TGF-β signaling, p53-72R induced p21 more efficiently than p53-72P, confirming the results shown in Fig. 5*D*. When ca. TGF-βR was co-transfected with p53s, TGF-β-dependent up-regulation of p21 was observed, and this induction was significantly stronger in cells expressing p53-72R. Enhanced induction efficiency of p21 in p53-72R-expressing cells with or without ca. TGF-βR was also confirmed by quantitative real time PCR (supplemental Fig. S5*C*). The difference between variants was abolished when Ser to Ala conversions were introduced at Ser-6, showing that the difference in p21 induction was brought about from differences in Ser-6 phosphorylation levels (Fig. 5*E*). Collectively, these results indicate that Ser-6 phosphorylation is important for p53 transactivation activity under basal conditions and upon activation of TGF-β signaling, and enhanced Ser-6 phosphorylation in p53-72R results in stronger induction of p21.

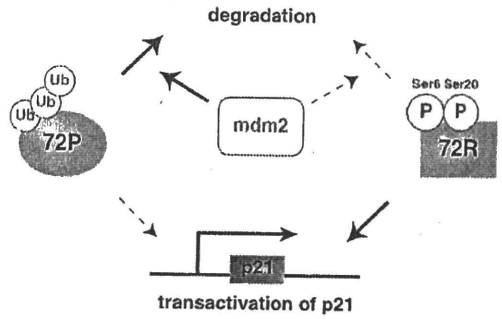

FIGURE 6. **Common polymorphism of p53 affects phosphorylation and degradation of p53 protein.** Phosphorylation of Ser-6 and -20 is enhanced in p53-72R compared with p53-72P. Difference in protein structure and phosphorylation of Ser-20 affects Mdm2-mediated degradation of p53 protein, whereas phosphorylation of Ser-6 affects transactivation ability of p53 protein.

DISCUSSION

The polymorphism of p53 at codon 72 is unique to humans and is very common. For example, 44% of Japanese are homozygous for p53-72R and 11% are homozygous for p53-72P (19). Cancer susceptibility and clinical outcome differ among individuals having the two variants; therefore, the impact of understanding the molecular basis for the difference between p53-72P and -72R is huge. Recently, using chimeric p53 protein containing N-terminal mouse p53 (amino acids 1–34) and human p53 (amino acids 32–393), it was shown that codon 72 polymorphism-specific effects of human p53 require N-terminal 31 amino acids of human p53 (26). In addition, we found that p53-72R and -72P proteins differ in structure, especially in the N-terminal region, by partial proteolytic digestion of the proteins. We speculated that differences in the protein structure may change the affinity of p53 variants with kinases that modify p53, especially in the N-terminal region, and we found that the variants differ in phosphorylation levels at Ser-6 and -20. We actually found that strength of association with Chk2 kinase differs between p53-72P and p53-72R (supplemental Fig. S6). We do not know the precise mechanism of the differential association of the variants with Chk2, and it is an interesting issue to clarify in future research.

It has been reported that p53 phosphorylated at Ser-20 escapes from degradation by Mdm2, leading to stabilization of the protein (6), whereas phosphorylation of Ser-6 is required for TGF-β-dependent induction of p21 and p15INK4b (25). We found that phosphorylation of these sites is enhanced in p53-72R, and consequently, the two p53 polymorphic variants differ in the stabilization of proteins and TGF-β-dependent and -independent induction of p21, both of which are important for the tumor-suppressive function of p53 (Fig. 6).

In this study, we have shown for the first time that the *mdm2* gene gain in tumors is more frequent in lung cancer cases homozygous for the p53-72P allele than with other genotypes. Although this association should be further validated in other sets of lung cancer cases, the present result demonstrates the possibility that p53-72P homozygotes develop lung cancer at a higher frequency upon gain of the *mdm2* gene and supports our data showing that p53-72P is more susceptible to Mdm2-mediated degradation. It will be interesting to determine whether such an association is also observed in patients with other types of cancer.

Previously, it was shown that the expression of p21 mRNA was altered by p53 codon 72 polymorphism, and the Pro allele variant was associated with decreased p21 mRNA levels compared with Arg allele (27). In this study, we have also shown that p21 expression was decreased in p53-72P compared with -72R and was dependent on p53 Ser-6 phosphorylation. The physiological relevance of Ser-6 phosphorylation remains unknown; however, it was shown recently to be required for TGF-β signaling. TGF-β is a potent growth inhibitor with tumor suppressing activity, and TGF-β-mediated growth suppression is mediated by p53 (28). TGF-β cooperates with p53 to induce p21, and this induction requires p53 to be phosphorylated at N-terminal Ser residues, including Ser-6 (25). We have shown that p53-72P was less phosphorylated at Ser-6 compared with p53-72R under all conditions studied, and TGF-β-dependent and -independent induction of p21 was attenuated in p53-72P-expressing cells. Previously, we have shown that phosphorylation of Ser-6 does not affect binding of p53 to p21 promoter (8). Therefore, Ser-6 may affect other aspects of p21 promoter activation, such as cofactor recruitment to the promoters.

The results shown in this study collectively reveal a novel difference in p53 polymorphic variants at codon 72. Although several molecular mechanisms to explain the difference in tumor suppression function of the variants have been reported, our results also reveal a novel difference in the variants through differences in protein structure and phosphorylation levels at Ser-6 and -20. Understanding the molecular mechanism leading to differences in the tumor suppression potential of the two variants is very important for cancer prevention and therapy. Our results may provide basic knowledge to develop novel cancer therapy or prevention strategies on the basis of the genotype of p53.

Acknowledgments—We thank Dr. Teruhiko Yoshida for providing immortalized peripheral lymphocytes. We also thank Dr. Yasumichi Inoue for providing pcDNA4-HisMax-Chk2 plasmid.

REFERENCES

1. Vogelstein, B., Lane, D., and Levine, A. J. (2000) *Nature* **408**, 307–310
2. Vousden, K. H., and Lu, X. (2002) *Nat. Rev. Cancer* **2**, 594–604
3. Braithwaite, A. W., and Prives, C. L. (2006) *Cell Death Differ.* **13**, 877–880
4. Prives, C. (1998) *Cell* **95**, 5–8
5. Xu, Y. (2003) *Cell Death Differ.* **10**, 400–403
6. Bode, A. M., and Dong, Z. (2004) *Nat. Rev. Cancer* **4**, 793–805
7. Oda, K., Arakawa, H., Tanaka, T., Matsuda, K., Tanikawa, C., Mori, T., Nishimori, H., Tamai, K., Tokino, T., Nakamura, Y., and Taya, Y. (2000) *Cell* **102**, 849–862
8. Kawase, T., Ichikawa, H., Ohta, T., Nozaki, N., Tashiro, F., Ohki, R., and Taya, Y. (2008) *Oncogene* **27**, 3797–3810
9. Kawase, T., Ohki, R., Shibata, T., Tsutsumi, S., Kamimura, N., Inazawa, J., Ohta, T., Ichikawa, H., Aburatani, H., Tashiro, F., and Taya, Y. (2009) *Cell* **136**, 535–550
10. Unger, T., Sionov, R. V., Moallem, E., Yee, C. L., Howley, P. M., Oren, M., and Haupt, Y. (1999) *Oncogene* **18**, 3205–3212
11. Toledo, F., and Wahl, G. M. (2006) *Nat. Rev. Cancer* **6**, 909–923
12. Zilfou, J. T., Hoffman, W. H., Sank, M., George, D. L., and Murphy, M. (2001) *Mol. Cell. Biol.* **21**, 3974–3985
13. Bergamaschi, D., Samuels, Y., Sullivan, A., Zvelebil, M., Breyssens, H., Bisso, A., Del Sal, G., Syed, N., Smith, P., Gasco, M., Crook, T., and Lu, X. (2006) *Nat. Genet.* **38**, 1133–1141
14. Harris, N., Brill, E., Shohat, O., Prokocimer, M., Wolf, D., Arai, N., and Rotter, V. (1986) *Mol. Cell. Biol.* **6**, 4650–4656
15. Murphy, M. E. (2006) *Cell Death Differ.* **13**, 916–920
16. Matlashewski, G. J., Tuck, S., Pim, D., Lamb, P., Schneider, J., and Crawford, L. V. (1987) *Mol. Cell. Biol.* **7**, 961–963
17. Soussi, T., and Wiman, K. G. (2007) *Cancer Cell* **12**, 303–312
18. Fan, R., Wu, M. T., Miller, D., Wain, J. C., Kelsey, K. T., Wiencke, J. K., and Christiani, D. C. (2000) *Cancer Epidemiol. Biomarkers Prev.* **9**, 1037–1042
19. Sakiyama, T., Kohno, T., Mimaki, S., Ohta, T., Yanagitani, N., Sobue, T., Kunitoh, H., Saito, R., Shimizu, K., Hirama, C., Kimura, J., Maeno, G., Hirose, H., Eguchi, T., Saito, D., Ohki, M., and Yokota, J. (2005) *Int. J. Cancer* **114**, 730–737
20. Boldrini, L., Gisfredi, S., Ursino, S., Lucchi, M., Greco, G., Mussi, A., and Fontanini, G. (2008) *Oncol. Rep.* **19**, 771–773
21. Tommiska, J., Eerola, H., Heinonen, M., Salonen, L., Kaare, M., Tallila, J., Ristimäki, A., von Smitten, K., Aittomäki, K., Heikkilä, P., Blomqvist, C., and Nevanlinna, H. (2005) *Clin. Cancer Res.* **11**, 5098–5103
22. Ohki, R., Kawase, T., Ohta, T., Ichikawa, H., and Taya, Y. (2007) *Cancer Sci.* **98**, 189–200
23. Okamoto, K., Kashima, K., Pereg, Y., Ishida, M., Yamazaki, S., Nota, A., Teunisse, A., Migliorini, D., Kitabayashi, I., Marine, J. C., Prives, C., Shiloh, Y., Jochemsen, A. G., and Taya, Y. (2005) *Mol. Cell. Biol.* **25**, 9608–9620
24. Shibata, T., Uryu, S., Kokubu, A., Hosoda, F., Ohki, M., Sakiyama, T., Matsuno, Y., Tsuchiya, R., Kanai, Y., Kondo, T., Imoto, I., Inazawa, J., and Hirohashi, S. (2005) *Clin. Cancer Res.* **11**, 6177–6185
25. Cordenonsi, M., Montagner, M., Adorno, M., Zacchigna, L., Martello, G., Mamidi, A., Soligo, S., Dupont, S., and Piccolo, S. (2007) *Science* **315**, 840–843
26. Phang, B. H., and Sabapathy, K. (2007) *Oncogene* **26**, 2964–2974
27. Su, L., Sai, Y., Fan, R., Thurston, S. W., Miller, D. P., Zhou, W., Wain, J. C., Lynch, T. J., Liu, G., and Christiani, D. C. (2003) *Lung Cancer* **40**, 259–266
28. Cordenonsi, M., Dupont, S., Maretto, S., Insinga, A., Imbriano, C., and Piccolo, S. (2003) *Cell* **113**, 301–314

Revision for Ms# 201009126R: Submission date, April 18, 2011

Phosphoinositide 3-kinase signaling pathway mediated by p110α regulates invadopodia formation

Hideki Yamaguchi[1, 2, 3, *], Shuhei Yoshida[2], Emi Muroi[1, 2], Nachi Yoshida[1, 2], Masahiro Kawamura[2], Zen Kouchi[2], Yoshikazu Nakamura[2], Ryuichi Sakai[1], and Kiyoko Fukami[2]

[1] Division of Metastasis and Invasion Signaling, National Cancer Center Research Institute, 5-1-1 Tsukiji, Chuo-ku, Tokyo 104-0045, Japan

[2] Laboratory of Genome and Biosignal, Tokyo University of Pharmacy and Life Sciences, 1432-1 Horinouchi, Hachioji, Tokyo 192-0392, Japan

[3] PRESTO (Precursory Research for Embryonic Science and Technology), Japan Science and Technology Agency, 4-1-8 Honcho, Kawaguchi, Saitama 332-0012, Japan

[*] **Corresponding author:**

Dr. Hideki Yamaguchi

Division of Metastasis and Invasion Signaling, National Cancer Center Research Institute, 5-1-1 Tsukiji, Chuo-ku, Tokyo 104-0045, Japan

Tel +81-3-3542-2511(ext. 4302), Fax +81-3-3542-8170, E-mail: hidyamag@ncc.go.jp

Running title: PI3-kinase p110α regulates invadopodia formation

Character count: 38028

Key words: Breast cancer/invadopodia/phosphoinositide 3-kinase/p110α/Akt

Abstract

Invadopodia are extracellular matrix-degrading protrusions formed by invasive cancer cells and are thought to function in cancer invasion. Although many invadopodia components have been identified, signaling pathways that link extracellular stimuli to invadopodia formation remain largely unknown. We investigated the role of phosphoinositide 3-kinase (PI3K) signaling during invadopodia formation. We found that in human breast cancer cells, both invadopodia formation and degradation of a gelatin matrix were blocked by treatment with PI3K inhibitors or sequestration of D-3 phosphoinositides. Functional analyses revealed that among the PI3K family proteins, the class I PI3K catalytic subunit p110α, a frequently mutated gene product in human cancers, is selectively involved in invadopodia formation. The expression of p110α with cancerous mutations promoted invadopodia-mediated invasive activity. Furthermore, inhibition of PDK1 and Akt, the downstream effectors of PI3K signaling, suppressed invadopodia formation induced by the p110α mutants. These data suggest that the PI3K signaling pathway via p110α regulates invadopodia-mediated invasion of breast cancer cells.

Introduction

Degradation of extracellular matrix (ECM) that is present in the basement membrane and tumor stroma is essential for local invasion and formation of metastatic sites by malignant cancer cells (Kessenbrock et al., 2010). Invadopodia, which were first described by Chen et al. (Chen, 1989), are ECM-degrading membrane protrusions formed on the ventral surface of invasive cancer cells and are thought to play a role in cancer cell invasion (Buccione et al., 2009; Madsen and Sahai, 2010; Weaver, 2006; Yamaguchi et al., 2005b). Invadopodia have been observed in a variety of invasive cancer cell lines, including mammary adenocarcinoma, colon carcinoma, melanoma, and glioma, as well as in primary invasive tumor cells derived from glioblastoma and head and neck cancers (Clark et al., 2007; Stylli et al., 2008). In the case of breast cancer cell lines, the ability to form invadopodia is closely related to their invasive and metastatic properties *in vivo* (Coopman et al., 1998; Yamaguchi et al., 2005a; Yamaguchi et al., 2009). Additionally, invadopodia-like protrusions in breast cancer cells have been observed during intravasation by intravital imaging (Condeelis and Segall, 2003; Yamaguchi et al., 2005b). A recent report showed that invasive cancer cells use invadopodia to breach the basement membrane and penetrate into the stroma (Schoumacher et al.). Moreover, Eckert et al. recently reported that Twist, an inducer of epithelial-mesenchymal transition, induces invadopodia formation to promote tumor metastasis and provided evidence of invadopodia formation *in vivo* in sections of invasive primary tumors (Eckert et al., 2011).

Many components of invadopodia, such as various proteins involved in actin polymerization, cell signaling, membrane trafficking, cell-ECM adhesion, and ECM degradation, have been reported to date (Caldieri and Buccione, 2010; Gimona et al.,

2008; Linder, 2007). We and other researchers previously reported that invadopodia formation is induced by stimulation with serum and growth factors (Tague et al., 2004; Yamaguchi et al., 2005a; Mandal et al., 2008; Eckert et al., 2011). However, the signaling pathways that link these extracellular stimuli to invadopodia formation remain largely unknown.

The phosphoinositide 3-kinases (PI3Ks) are a family of lipid kinases that phosphorylate phosphoinositides at the D-3 position of the inositol headgroup and thus produce D-3 phosphoinositides (Cantley, 2002). PI3Ks mediate the signal transduction of extracellular stimuli and regulate diverse cellular events, such as mitogenesis, survival, membrane transport, and cell migration (Cain and Ridley, 2009; Engelman et al., 2006). PI3Ks are subdivided into three general classes (I–III) in mammals on the basis of their enzyme domain structures and substrate specificities (Fruman et al., 1998). Specifically, the class I subfamily consists of four catalytic subunits, including three class IA subunits (p110α, p110β, and p110δ) and a single class IB subunit (p110γ). However, the class II PI3K group consists of three isoforms, PI3K-C2α, PI3K-C2β, and PI3K-C2γ. Finally, mammals have a single class III isoform, namely, Vps34, which is a homolog of the sole PI3K present in yeast.

Uncontrolled activation of the PI3K signaling pathway leads to several pathological phenomena, including tumorigenesis and tumor malignancy (Cantley, 2002). This is evidenced by the finding that the expression and activity of several members of the PI3K signaling pathway are frequently altered in a variety of human cancers (Yuan and Cantley, 2008). For instance, the *PIK3CA* gene, which encodes the class IA PI3K catalytic subunit p110α, is one of the most frequently amplified and mutated genes identified in human cancers (Yuan and Cantley, 2008; Zhao and Vogt, 2008). Clinical studies involving human breast cancer patients revealed that mutations

leading to the activation of *PIK3CA* are associated with the development of invasive and metastatic phenotypes and poor patient prognosis (Li et al., 2006; Maruyama et al., 2007; Saal et al., 2005). Moreover, a previous study has shown that introduction of the mutant *PIK3CA* gene into a breast cancer cell line enhanced lung metastasis in mice (Pang et al., 2009). However, the detailed mechanisms by which the *PIK3CA* gene product p110α contributes to cancer invasion and metastasis are yet to be determined.

It is established that 3-phosphoinositide-dependent protein kinase-1 (PDK1) is a serine/threonine kinase that mediates PI3K signaling during various cellular responses (Toker and Newton, 2000). PDK1 is recruited to cell membranes upon PI3K activation, where it phosphorylates and activates Akt, the major mediator of the PI3K signaling pathway (Stephens et al., 1998). Both PDK1 and Akt are overexpressed in human breast cancers and are thought to be critical components of the oncogenic PI3K signaling pathway (Dillon et al., 2007; Maurer et al., 2009; Sheng et al., 2009). Furthermore, previous studies have demonstrated that PDK1 and Akt are involved in the invasive and metastatic phenotypes of human cancer cells (Dillon et al., 2007; Liu et al., 2009; Sheng et al., 2009; Xie et al., 2006). However, the roles of PDK1 and Akt in invadopodia formation remain unclear. In the present study, we investigated the role of PI3K signaling during invadopodia formation in invasive human breast cancer cells.

Results

PI3K activity is required for invadopodia formation in human breast cancer cells

The formation of invadopodia in human cancer cells and podosomes, which are structures functionally similar to invadopodia, in Src-transformed fibroblasts requires the activity of PI3K (Mandal et al., 2008; Nakahara et al., 2003; Oikawa et al., 2008). In the present study, the role of PI3K in invadopodia formation was investigated in detail in the highly invasive human breast cancer cell line MDA-MB-231 (Neve et al., 2006). MDA-MB-231 cells form invadopodia *in vitro* and have therefore been widely used in studies investigating various aspects of these invasive structures. MDA-MB-231 cells were seeded onto fluorescent gelatin-coated coverslips in the presence or absence of each of two PI3K inhibitors, LY294002 and wortmannin, and stained for two invadopodia markers, cortactin and F-actin. Invadopodia were observed as dot-like clusters of cortactin and F-actin on the ventral membrane of cells, which corresponded with the degradation sites on the gelatin matrix (Supplementary Figure S1A). To quantify the invadopodia-mediated degradation of the gelatin matrix for each treatment, we calculated the area of the degradation sites. Both LY294002 and wortmannin significantly inhibited the formation of invadopodia and gelatin degradation in a dose-dependent manner, with IC_{50} values of 3.7 μM and 3.5 nM for LY294002 and wortmannin, respectively (Supplementary Figure S1B–D). Furthermore, the percentage of cells with invadopodia and the number of invadopodia per cell were also reduced in cells treated with either PI3K inhibitor (Supplementary Figure S1E and F).

We also examined the effect of PI3K inhibition on the stability of preformed invadopodia. MDA-MB-231 cells expressing GFP-actin were seeded onto plates coated with a gelatin matrix, and cells were observed using time-lapse microscopy

upon treatment with LY294002. LY294002 treatment of cells exhibiting GFP-actin-positive invadopodia resulted in the degradation of invadopodia within 1 min of treatment (Supplementary Figure S1G; Supplementary Video 1). A similar result was obtained when cells expressing Venus-cortactin were analyzed in the same manner (Supplementary Video 2). Quantification of the intensity of GFP-actin signals at the invadopodia revealed that the actin core structures of invadopodia disassembled immediately after the addition of LY294002, whereas the invadopodia of cells treated with dimethylsulfoxide (DMSO) did not disassemble (Supplementary Figure S1H). Collectively, these results indicate that PI3K activation is required for both the formation and stability of invadopodia in human breast cancer cells.

D-3 phosphoinositides are required for invadopodia formation

We next investigated the role of D-3 phosphoinositides synthesized by PI3Ks in invadopodia formation. The pleckstrin-homology (PH) domain of Akt interacts with $PI(3,4,5)P_3$ and $PI(3,4)P_2$, which are two major products of PI3K, and its overexpression results in the sequestration and inhibition of the function of these phosphoinositides (Varnai et al., 2005). In the present study, the PH domain of Akt was overexpressed in MDA-MB-231 cells as a GFP-fusion protein (GFP-Akt-PH). This construct, which localized to the plasma membrane, inhibited the formation of invadopodia, as measured by both the percentage of cells with invadopodia and the number of invadopodia per cell, and gelatin degradation (Figure 1A–D). In contrast, a mutant form of the Akt PH domain (R25C), in which an essential amino acid for phosphoinositide binding is mutated (Varnai et al., 2005), did not localize to the plasma membrane or inhibit gelatin degradation (Figure 1A and B). Furthermore, to examine the localization of D-3 phosphoinositides at invadopodia sites, a cell line